Scripta Materialia 205 (2021) 114177

Contents lists available at ScienceDirect

Scripta Materialia

journal homepage: www.elsevier.com/locate/scriptamat

Predicting the energetics and kinetics of Cr atoms in Fe-Ni-Cr alloys via physics-based machine learning

Yuchu Wang[a], Bita Ghaffari[b], Christopher Taylor[c], Simon Lekakh[d], Mei Li[b], Yue Fan[a,*]

[a] Department of Mechanical Engineering, University of Michigan, Ann Arbor, MI 48109, USA
[b] Ford Research and Advanced Engineering, Ford Motor Company, Dearborn, MI 48124, USA
[c] Department of Materials Science and Engineering, Ohio State University, Columbus, OH 43210, USA
[d] Department of Materials Science and Engineering, Missouri University of Science and Technology, Rolla, MO 65409, USA

ARTICLE INFO

Article history:
Received 1 April 2021
Revised 18 June 2021
Accepted 27 July 2021

ABSTRACT

The energy and activation barrier distributions of Cr atoms in austenitic alloys are investigated over a multiplicity of modeling samples across a wide range of chemical (*e.g.* solid solutions *vs.* segregated states) and microstructural (*e.g.* bulk *vs.* grain boundaries) environments. Assisted with a physics-based machine learning algorithm, it is found that the thermodynamic and kinetic behaviors of Cr atoms can be reliably predicted according to the local electronegativity (χ) and free volume of local atomic packing (V_v). The corresponding predictive maps in the $\chi - V_v$ parameter space are established, which are in line with existing experiments and validated by a parallel modeling with a different interatomic force field. The implications of the present study regarding its potential to guide the design of austenitic alloys with desired properties are also discussed.

Superior mechanical properties and strong resistance to corrosion have endowed Cr-Ni austenitic stainless steels with great performance potential in many applications [1] across the transport, energy, and manufacturing sectors. The chemical element distributions in the alloys are rarely uniform. For example, Cr atoms tend to segregate near grain boundaries (GBs) or surfaces [2-6]. It has been shown that such a heterogeneous spatial distribution of elements plays a significant role in the initiation of oxidations [2,3,7], which may consequently affect the materials' mechanical performance [8-11], such as high-temperature fatigue, creep, stress corrosion cracking, *etc*. Therefore, a fundamental understanding of Cr atoms' energetics and kinetics in Fe-Ni-Cr alloys is of crucial importance.

While the subject has been probed by numerous studies [6,7,12-17], a predictive knowledge on the stability and mobility of Cr in the alloys is still lacking at the atomic level, mainly due to the system's chemical heterogeneity and microstructural complexity (*e.g.* the presence of disordered GBs). Machine learning (ML), as an emerging powerful technique, has recently been utilized to study multi-element and disorder-containing alloys [18-21]. However, many of the existing ML practices are either (i) focused on predicting the average properties of the entire system rather than the local details in the presence of chemical and structural heterogeneities, or (ii) built in the manners of essentially black-box algorithms, therefore lacking an interpretability and obstructing the physical insights one can learn and eventually apply to the design of alloys.

In the present study, we report a physics-based ML study that allows one to reliably predict the energy and activation barrier of individual Cr atoms in Fe-Ni-Cr alloys across a broad range of local environments with various compositions (*e.g.* from solid solutions to highly segregated states) and microstructures (*e.g.* from bulk to GBs at various misorientations). Different from conventional ML practices, in the present study, the training and prediction of ML algorithm is built in a parameter space with explicit physical meaning, namely the local electronegativity and atomic packing topology (*e.g.* Voronoi cell volume). It is found that the Cr atoms' thermodynamic stability is more sensitive to their local electronegativity, while their kinetic mobility is more responsive to the local atomic packing, according to which two corresponding quantitative contour maps are established. Since the parameter space hereby adopted can be controlled in experiments by compositional tuning, choice of manufacturing, and mechanical processing, the insights obtained in the present study might therefore shed light on the design of austenitic alloys with desired properties.

To study the distributions and energetics of Cr atoms over a broad range of chemical and physical environments, we built a multiplicity of GB-containing Fe-Ni-Cr model samples at various

* Corresponding author.
E-mail address: fanyue@umich.edu (Y. Fan).

https://doi.org/10.1016/j.scriptamat.2021.114177
1359-6462/

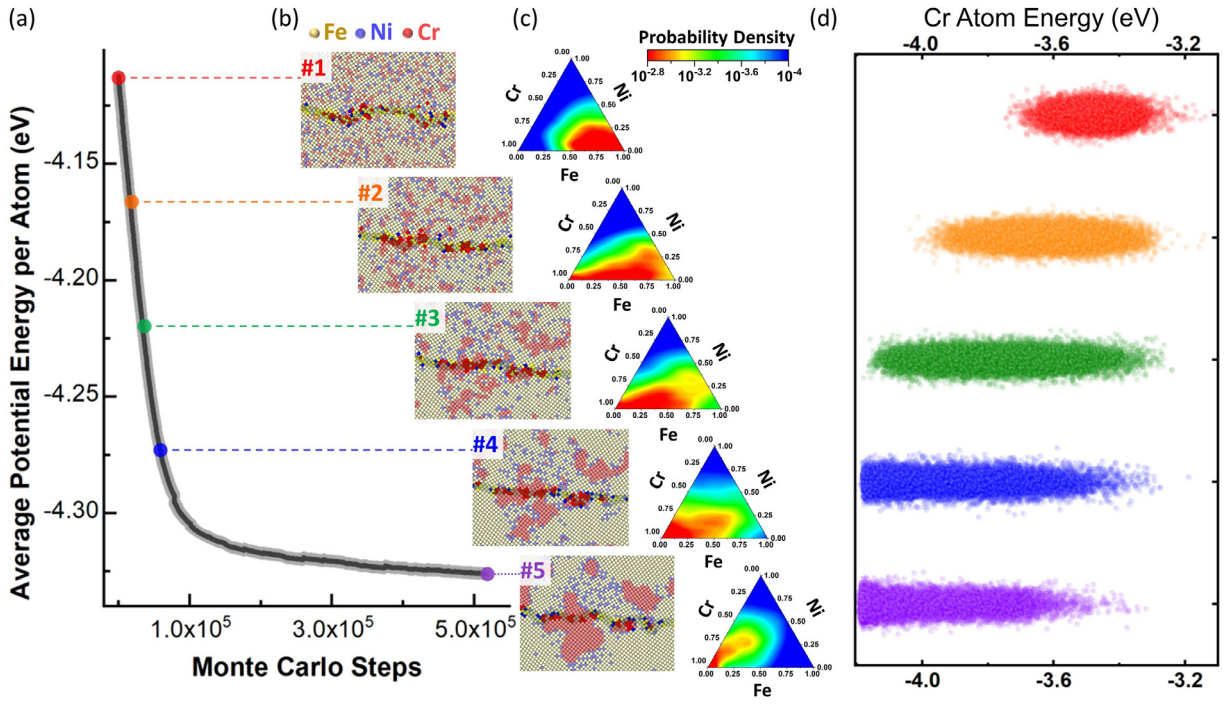

Fig. 1. (a) Energy curve and (b) microstructural evolution of a Σ25 (710) bi-crystal $Fe_{70}Ni_{10}Cr_{20}$ system during MC metropolis algorithm. (c) The corresponding local chemical environment of Cr atoms in ternary plots. (d) Distributions of Cr atoms' energy in the selected states.

compositions and GB-misorientation angles. In particular, a group of symmetric tilt <100> GBs are created following the widely used bi-crystal set-up protocol [22,23]. An embedded atom method (EAM) interatomic potential [24] calibrated to first-principles calculations is employed, and to be compatible with the applied periodic boundary conditions the primary focus is placed on the coincident site lattice (CSL) GBs. The initial states of the samples are set as solid solutions, by randomly assigning Fe, Cr, and Ni atoms to the lattice sites. A Monte Carlo (MC) metropolis algorithm is then applied to explore the thermodynamically favorable states. As seen in Figs. 1**-a & b**, which correspond to MC simulation of a $Fe_{70}Ni_{10}Cr_{20}$ system, Cr-segregated states are energetically more stable than the random solid-solution state, corroborating experimental evidence [4] and others' previous calculations [6]. Fig. 1**-c** shows the distributions of local composition near individual Cr atoms (within 1st-nearest neighbors) in a few selected states in the system, clearly demonstrating the wide fluctuations of local chemical environments. The corresponding energy of Cr atoms also varies significantly by more than 1 *eV*, as marked in Fig. 1**-d**. These calculated energies are utilized in the ML training and testing discussed below.

The kinetic mobility of an atom is determined by the activation barrier of the collective rearrangements of the atom and its surrounding particles, which correspond to hopping between neighboring local minima in the system's underlying potential energy landscape (PEL) [25-27]. In the present study, we employ the activation relaxation technique (ART) [28,29] to probe the PEL and thus identify the E_A distributions of Cr atoms.

More specifically, given a Cr atom of interest, small random perturbations are introduced to it and its 1st-nearest neighbors to initiate the ART algorithm [30] which drives the system moving uphill along the PEL. The 1st-nearest neighbor cutoff radius is defined according to the first dip of the radial distribution function, which is about 3 Å both in GBs and in the bulk (see Supplemental Materials). The inflection point is reached when the smallest eigenvalue of the PEL's Hessian matrix becomes negative (practically less than -0.01 $eV/Å^2$), and the system is then relaxed to the saddle point at the criterion when the net force is smaller than 0.005 *eV/Å*. The energy difference between the identified saddle state and the initial state in the PEL is thus the activation barrier. Note that the same atom can be involved in several different hopping events, and therefore in the present study each selected Cr atom is exposed to many ART searches with different random perturbations to ensure sufficient statistics. The hereby calculated E_A distributions are then utilized in the following ML training and testing. We would like to note that, accompanied with the broad E_A spectra there are numerous atomic rearrangement mechanisms, due to both the chemical heterogeneity and microstructural complexity. On the other hand, the primary focus of this study is to get a predictive and quantitative assessment on Cr atoms' kinetic mobility, and therefore in the below discussions we are more concentrated in the activation barriers instead of the detailed rearrangement mechanisms.

To obtain interpretable knowledge, the ML algorithm in the present study is built in a parameter space with explicit physical meaning. In particular, we adopt a parameter space spanned by local electronegativity and local free volume, because of their reported correlations [31-33] with the properties of multi-component and disorder-containing alloys. Specifically, the local electronegativity in the vicinity of a given atom is defined as the convolution of a radial Gaussian weight and the electronegativity of its surrounding atoms, $\langle \chi_i \rangle \equiv [\sum_j \exp(-\frac{r_{ij}^2}{2\sigma^2})\chi_j]/\sum_j \exp(-\frac{r_{ij}^2}{2\sigma^2})$, where σ is set as 3.0 *Å*, corresponding to the first dip of radial distribution function [32]. The local free volume of a given atom, defined as V_v, is characterized by the polyhedral volume following a Voronoi tessellation. The hereby defined $\langle \chi_i \rangle$ and V_v essentially represent the local chemical environment, and local physical packing, respectively.

In the ML training, either the Cr atom's energy or E_A is used as the supervisory signal y_i. A standard regularized least squares (RLS) regression [18] is employed in the present study to identify

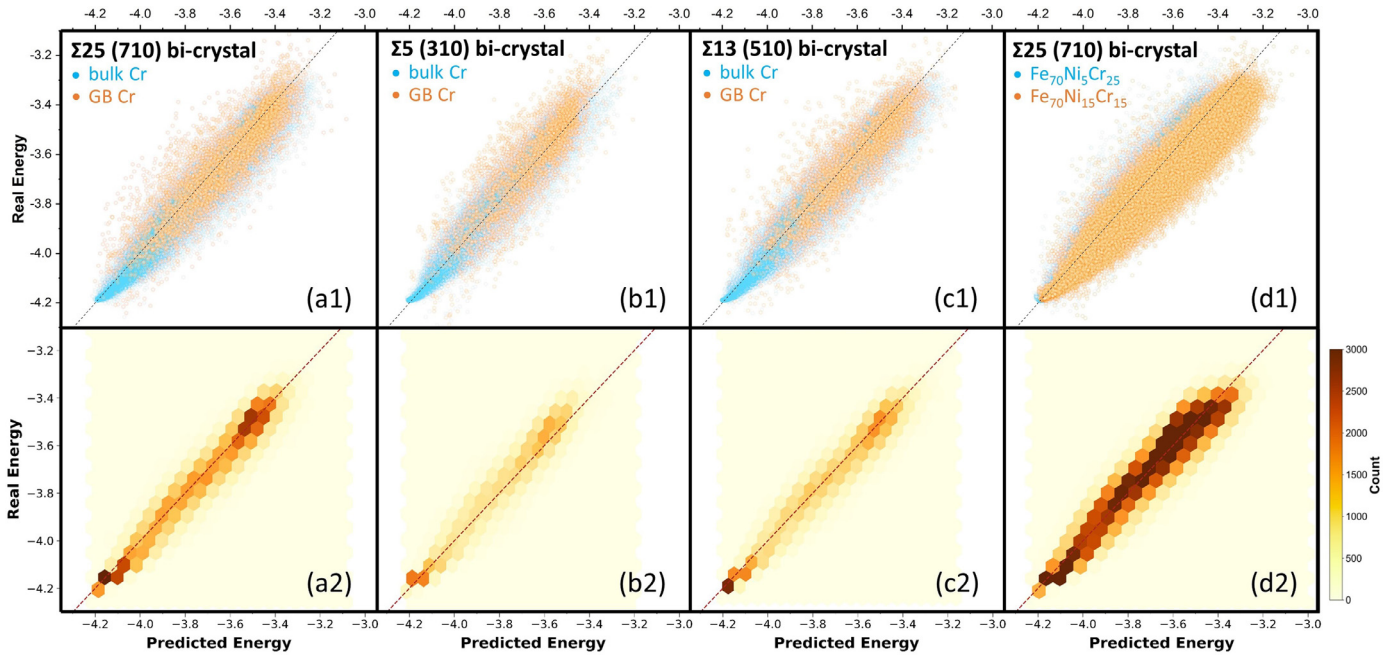

Fig. 2. The ML prediction of the energy of Cr atoms compared to the real energy in (a) Σ25 (710) bi-crystal system, (b) Σ5 (310) bi-crystal system, (c) Σ13 (510) bi-crystal system, and (d) $Fe_{70}Ni_5Cr_{25}$ and $Fe_{70}Ni_{15}Cr_{15}$ systems.

the weight vector ω that can minimize the L2 regularization loss of all the training Cr atoms:

$$\omega^* = \min_{\omega} ||y - \boldsymbol{X}\omega||_2^2 + \lambda||\omega||_2^2 \quad (1)$$

where y is the supervisory signal vector, $\boldsymbol{X}$ is a matrix with each row to be the feature vector of *i-th* atoms in the grand $\chi - V_\nu$ space and $\lambda \geq 0$ is the regularization parameter. The optimal weight vector ω^* hereby obtained through the ML algorithm is then used for the later testing and prediction.

We first study the ML prediction of Cr atom energy. The training dataset is selected from the Σ25 (710) GB system shown above in Fig. 1 at the composition of $Fe_{70}Ni_{10}Cr_{20}$. More specifically, among the total 80,160 Cr atoms in the five states selected during the MC simulation, partial data from samples #1 and #5 are randomly selected as the training set, consisting of 20% of the total data. The remaining 80% of the data serves as the testing set. Other testing scenarios at various compositions and GB angles are also considered, where no more training is employed and all the data are used for testing.

Fig. 2-**a1** shows the comparison between ML-predicted Cr atoms' energy and the directly calculated result (will be referred to as the real value henceforth) in Σ25 (710) GB system. Note that this panel includes both the training and testing data mentioned above. It can be seen that the ML predictions and real values present good alignment, and it is worth noting that the Cr atoms near GBs, where significant disorders exist, are also well predicted. Fig. 2-**a2** shows the density plot of all the data points, and it is clear that the vast majority of data are located on the diagonal line, indicating the robustness of the ML training.

Fig. 2-b & c show the ML predictions of Cr atoms' energy in two other different GBs at Σ5 (310), and Σ13 (510), respectively, at the same composition as Fig. 2-a. Fig. 2-d presents the ML predictions for compositions of $Fe_{70}Ni_5Cr_{25}$, and $Fe_{70}Ni_{15}Cr_{15}$, while retaining the GB structure as Σ25 (710). Note that all the data points in Fig. 2-b to 2-d are testing data, and the high Pearson correlation coefficients marked in the plots demonstrate that the hereby ML-trained model can reliably predict the Cr atoms' energy over a broad range of chemical environments (from solid solutions to highly segregated states at different compositions) and microstructures (from bulk to GBs at various misorientations).

We would like to note that the partition of training vs. testing in the present study is much smaller than the 80% : 20% in many existing practices. It is worth emphasizing that there are no specific rules on how to partition the training set and testing set. In principle, maintaining the same level of prediction accuracy while using a smaller amount of training data is a reliable indication of the robustness of the model. Therefore, the very high Pearson correlation coefficient (ρ>0.95) by using only 20% of the training data suggests that our ML model captures the essence of the underlying physics.

We then focus on the ML prediction on E_A distributions of Cr atoms. Exploring the PEL and probing the activation barriers are computationally much more expensive than the simple energy calculation, and we therefore slightly narrow the scope in this task. More specifically, 70% of data points in sample #5, namely the Cr-segregated state of the Σ25 (710) GB system in Fig. 1-**b**, are employed for the ML training. The trained model is then used to test other samples at different chemistries (*e.g.* random solid-solution state) and GB angles.

Different from the energetics calculations, where a given atom has an explicitly defined energy, in kinetics the same atom can participate in multiple rearrangement events, and therefore a point-to-point correlation plot akin to Fig. 2 is not applicable here. Instead, a more suitable practice [18] is to contrast the E_A spectra between the predicted most mobile atoms and most sessile atoms. If the real calculated E_A spectra can be well separated by the ML predictions for the same atoms, then the ML training/prediction is regarded as successful and *vice versa*.

Fig. 3-**a** shows the real E_A distributions of those Cr atoms that fell into the bottom and top 10% mobility predicted by ML in the Cr-segregated Σ25 (710) GB sample. Since this panel includes both training and testing data, the good separation between the two spectra is not surprising. Fig. 3-**b** shows the ML-predicted results for the same GB sample but in a random solid-solution state; while Fig. 3-**c & d** show the predictions for a different Σ5 (310) GB system at a Cr-segregated state, and a solid-solution state, respec-

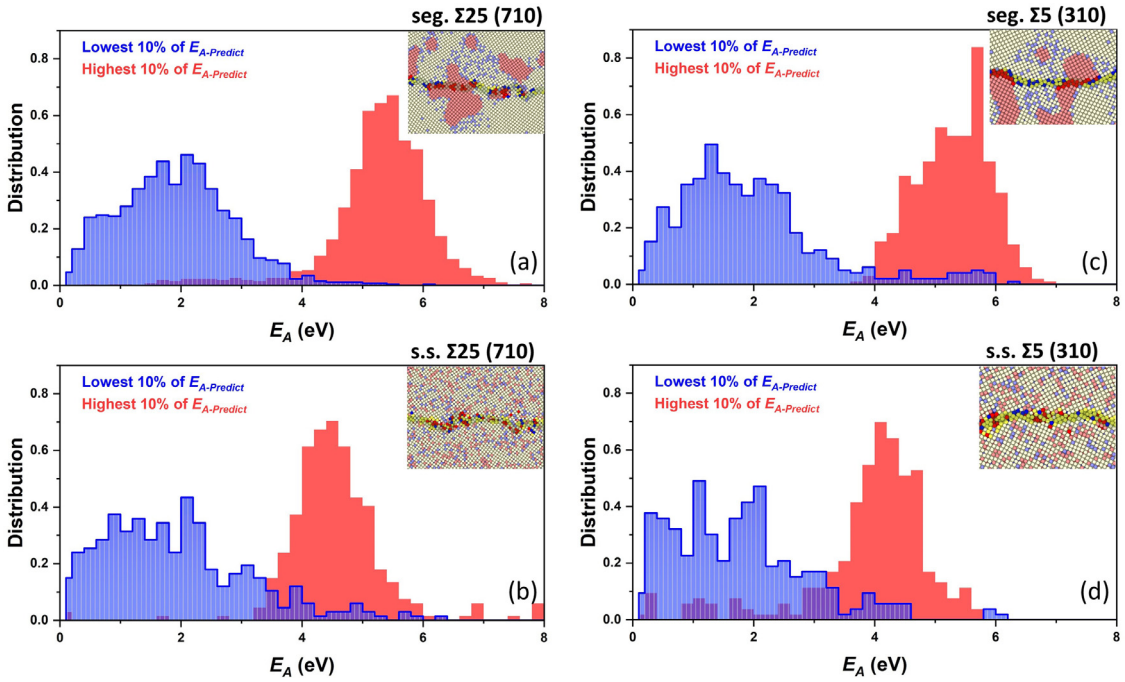

Fig. 3. The real E_A distributions of those Cr atoms with ML-predicted bottom and top 10% mobility in (a) segregated Σ25 (710) bi-crystal system, (b) random solid solution Σ25 (710) bi-crystal system, (c) segregated Σ5 (310) bi-crystal system, and (d) random solid solution Σ5 (310) bi-crystal system.

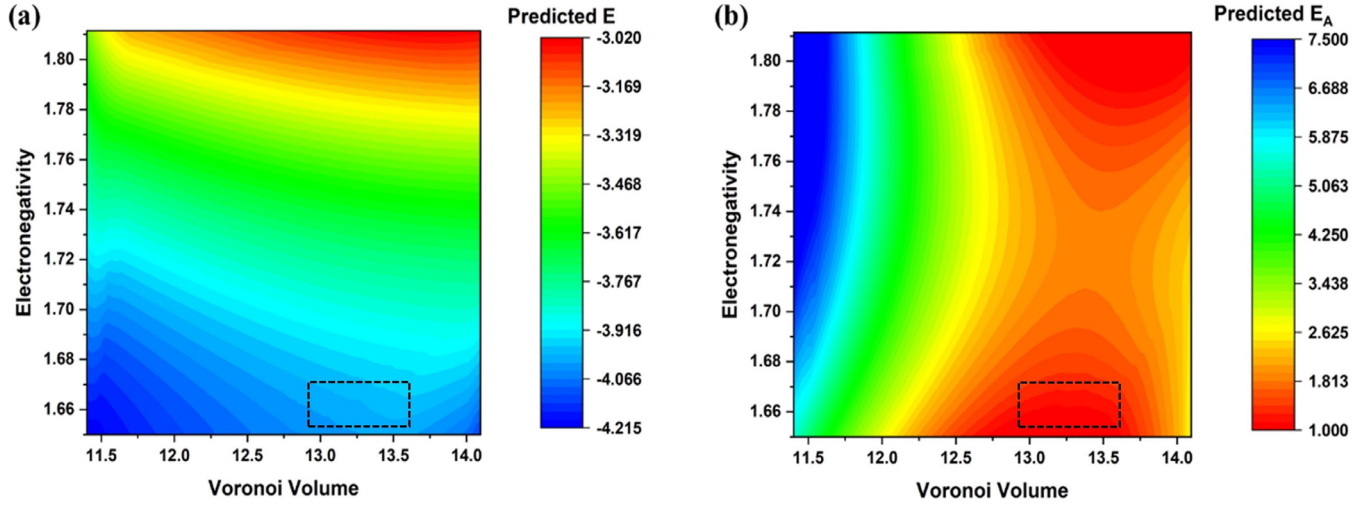

Fig. 4. ML-predicted (a) energy and (b) activation barrier of Cr atoms in austenitic Fe-Ni-Cr alloys in the parameter space spanned by local electronegativity and local free volume. The ML-trained analytical expressions for the predicted E and E_A are provided in Supplementary Materials.

tively. Note that there are no further trainings in these 3 panels, and the clear spectra contrasts validated by real ART calculations are remarkable, indicating a strong predictive power on the kinetic behavior of Cr atoms in Fe-Ni-Cr alloys.

It is also worth noting that the selection of top- and bottom-10% windows follows the common practice in similar problems [18], and there is actually no specific limitation on the window sizes. We have tested other window sizes at 5% and 20%, respectively, and no qualitative differences are observed (see Supplemental Materials).

Results in Figs. 2-3 suggest that the ML model in the present study is reliable and robust. In addition, since the ML training has been conducted in a physics-based parameter space, we can therefore plot the ML-predicted energetics and effective EA in the $\chi - V_v$ space as seen below in Fig. 4. Note that Fig. 4 spans a very wide range of the parameter space covering all the local environments of Cr atoms in the present study, including both solid-solution states and segregated states, as well as both GBs and bulk (e.g. when V_v is below about 11.75 Å^3).

Specifically, Fig. 4**-a** reveals that a smaller local Voronoi volume, as well as a smaller local electronegativity, can help improve Cr's thermodynamic stability, but χ shows a much larger sensitivity than V_v does. However, for the kinetic property, Fig. 4**-b** shows that V_v has a larger impact than χ does. Since a sample's electronegativity and atomic volume can be harnessed in experiments by composition tuning, choices of manufacturing, and/or mechanical processing, the maps in Fig. 4**-a & b**, therefore, can be combined to guide the design of austenitic alloys with desired thermodynamic and kinetic properties. For example, in the marked regime in Fig. 4 on the one hand, the energy of Cr atoms is relatively low, indicating thermodynamically more favorable states; on the other hand, the activation barriers are quite small, suggesting an

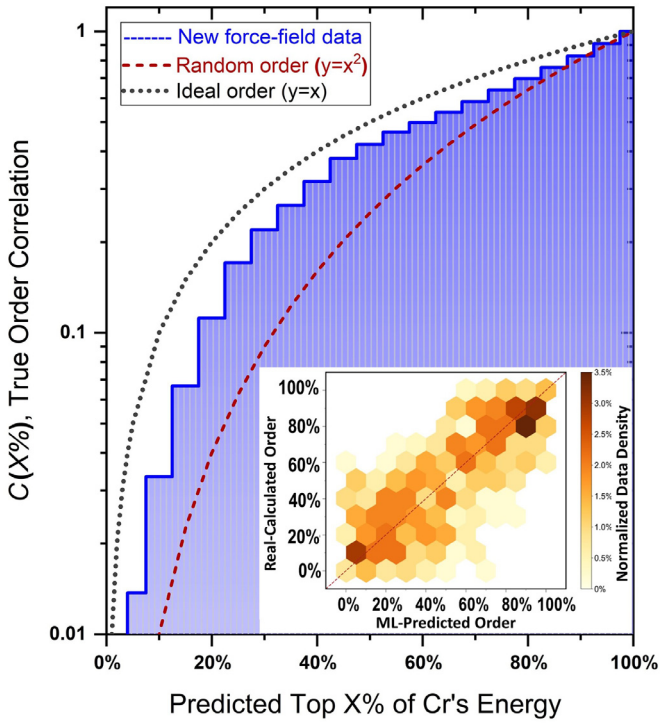

Fig. 5. Validation of the ML-predicted Cr atom energy using a different DFT-calibrated force field developed for Fe-Ni-Cr alloys.

enhanced transport or diffusion of Cr atoms. Remarkably, such an ML-predicted picture is in line with the reported measurements by Kim et al. [2]. To be more specific, given its relatively high-V_v and low-χ range, the marked regime in Fig. 4 should correspond to the Cr-segregated GBs environment. In Kim et al.'s experiments it has been reported that near the GBs a Cr_2O_3 protective layer is likely to present, while a Fe-rich non-protective layer would prevail away from the GBs intersections. The reason has been attributed to the enriched Cr distribution at GBs and the rapid diffusion of Cr along GBs [2], which is well consistent with our present results.

Another way of validating the ML-predicted Fig. 4 is to directly employ first-principles calculations such as density-functional theory (DFT) to accurately quantify the Cr's energetics at more complex local environments. However, the heavy computational cost and the consequently small simulation sizes in DFT make it practically very challenging to create a wide variety of local chemical and physical environments to match with the range in Fig. 4. As an alternative, we employ another EAM force field for austenitic Fe-Ni-Cr alloy [34] that has been extensively benchmarked against the DFT-calculated cohesive energy for different species. The idea is that, if the Cr's energy variation trend in Fig. 4-**a** can withstand the new force field system, then the correct physics should have been reflected in the hereby ML-trained model. Specifically, a solid-solution state of a Σ25 (710) bi-crystal $Fe_{70}Ni_{10}Cr_{20}$ is created with the new EAM potential, and the energies of randomly-selected Cr atoms from both bulk and GB are ranked according to the ML-predicted map in Fig. 4-**a**. Then their true ranking orders in the new force field are directly calculated and correlated with the ML-predicted orders, which shows a consistent trend as seen in the inset of Fig. 5. To further quantify such a correlation, we introduce a $C(X\%)$ function defined as:

$$C(X\%) \equiv f(i \in \{top\ X\%\ real\ energy\} | i \in \{top\ X\%\ predicted\ energy\}) \cdot X\% \quad (2)$$

where the first term estimates that, among those Cr atoms within the top $X\%$ energy window predicted by ML, what is the fraction that truly belongs to this window in the real calculations; while the second term is the corresponding normalization factor. For example, assume there are 1000 Cr atoms in the sample, and we select the 200 highest-energy atoms predicted by ML (*i.e.* x value of 20% in Fig. 5). And after direct energy calculation it is found that, say, only 150 out of those 200 atoms are truly within the top 20% energy window, then the y value in Fig. 5 is 150/1000=0.15.

One can easily prove two features of the above definition: (i) under the ideal scenario where the predicted order of each single Cr atom is correct, one should expect a $y=x$ theoretical profile (dotted black curve) in Fig. 5; and, (ii) under the other extreme where the ML prediction does not show any correlation with the real calculation, one should then expect a $y=x^2$ theoretical profile (dashed red curve). This is because, for example, among those 200 ML-predicted atoms mentioned above, only 20% of those (*i.e.* 40 atoms) should actually occupy a position in this window under a random distribution, meaning a y value of 0.04. It is evident in Fig. 5 that the predictive power remains robust in such a new system, suggesting that the correct physics has been effectively captured by the ML.

As a final remark, we have demonstrated that assisted with a physics-based ML study, the energetics and kinetics of Cr atoms in austenitic Fe-Ni-Cr alloys can be reliably predicted according to the local electronegativity and atomic packing environments. With the hereby constructed maps of Cr atom energy (E) and activation barrier (E_A), one can then in principle define an arbitrary performance function $f(E, E_A)$ tailored to a specific combination of thermodynamic and kinetic properties depending on the specific requirements in the application of interest. For instance, to design alloys against high-temperature creep it is desired that the system should simultaneously possess high thermodynamic stability and low kinetic mobility. Then according to Fig. 4-**a** and **b** one should focus on the middle-left region in the $\chi - V_v$ parameter space, which may be achieved by synergistically tuning the chemical composition (to change χ) and the physical processing (to change V_v). In other words, the non-linear maps would allow one to optimize a system's performance under certain constraints.

It is also worth noting that, while the quantitative patterns in Fig. 4 might be subject to change for other materials with different interatomic potentials, the methodology of the present study is quite general and not limited by the specific force fields. More specifically, the key physics reflected by this study is that the energetics and kinetics of alloys containing complex chemistries and microstructures can be reasonably predicted in light of the local electronegativity and atomic packing environments. Such a picture is in accordance with recent studies on a number of high-entropy alloys, which demonstrate that there are very strong correlations between the strength of the alloys and the electronegativity difference among the constituent elements [31]. Therefore, we believe the physics discovered in our present study and the methodology enabling the discovery are broadly applicable.

Declaration of Competing Interest

The authors declare that they have no known competing financial interests or personal relationships that could have appeared to influence the work reported in this paper.

Acknowledgement

The authors thank the University Research Program at Ford Motor Company, USA, for financial support. YF would also like to acknowledge that the grain boundaries' set up and analyses are based upon work support by NSF DMR-1944879.

Supplementary materials

Supplementary material associated with this article can be found, in the online version, at doi:10.1016/j.scriptamat.2021.114177.

References

[1] T. Michler, Reference Module in Materials Science and Materials Engineering, Elsevier, 2016.
[2] J.-H. Kim, et al., Corros. Sci. 96 (2015) 52–66.
[3] L. Ma, et al., Corros. Sci. 140 (2018) 205–216.
[4] H. Li, et al., J. Nucl. Mater. 439 (1) (2013) 57–64.
[5] E. Clauberg, et al., Appl. Surf. Sci. 161 (1) (2000) 35–46.
[6] X. Zhou, et al., Sci. Rep. 6 (1) (2016) 34642.
[7] M. Lampimäki, et al., J. Electron Spectrosc. Relat. Phenom. 154 (3) (2007) 69–78.
[8] R.W. Neu, H. Sehitoglu, Metall. Trans. A 20 (9) (1989) 1755–1767.
[9] R.W. Neu, H. Sehitoglu, Metall. Trans. A 20 (9) (1989) 1769–1783.
[10] V. Mazánová, M. Heczko, J. Polák, Int. J. Fatigue 114 (2018) 11–21.
[11] B. Li, et al., Mater. Sci. Eng. A 752 (2019) 1–14.
[12] T. Massoud, et al., Corros. Sci. 84 (2014) 198–203.
[13] L. Tan, et al., Mater. Sci. Eng. A 528 (6) (2011) 2755–2761.
[14] J. Zhou, et al., Scr. Mater. 75 (2014) 62–65.
[15] V.G. Gavriljuk, B.D. Shanina, H. Berns, Acta Mater. 48 (15) (2000) 3879–3893.
[16] R. Idczak, R. Konieczny, J. Chojcan, J. Phys. Chem. Solids 73 (9) (2012) 1095–1098.
[17] M. Liu, et al., J. Electrochem. Soc. 165 (11) (2018) C830–C834.
[18] Z. Fan, J. Ding, E. Ma, Mater. Today 40 (2020) 48–62.
[19] L. Tian, et al., Scr. Mater. 186 (2020) 185–189.
[20] Z. Zhou, et al., npj Comput. Mater. 5 (1) (2019) 128.
[21] S.Y. Lee, et al., Mater. Des. 197 (2021) 109260.
[22] M.A. Tschopp, S.P. Coleman, D.L. McDowell, Integr. Mater. Manuf. Innov. 4 (1) (2015) 176–189.
[23] Z. Bai, et al., Acta Mater. 200 (2020) 328–337.
[24] G. Bonny, N. Castin, D. Terentyev, Model. Simul. Mater. Sci. Eng. 21 (8) (2013) 085004.
[25] Y. Fan, B. Yildiz, S. Yip, Soft Matter 9 (40) (2013) 9511–9514.
[26] Y. Fan, T. Iwashita, T. Egami, Nat. Commun. 8 (2017) 15417.
[27] Z. Bai, Y. Fan, Phys. Rev. Lett. 120 (12) (2018) 125504.
[28] Y. Fan, T. Iwashita, T. Egami, Nat. Commun. 5 (2014) 5083.
[29] E. Cances, et al., J. Chem. Phys. 130 (11) (2009) 114711.
[30] G.T. Barkema, N. Mousseau, Phys. Rev. Lett. 77 (21) (1996) 4358–4361.
[31] H.S. Oh, et al., Nat. Commun. 10 (1) (2019) 2090.
[32] C.-H. Tung, et al., Mater. Sci. (2020).
[33] X.L. Bian, et al., Acta Mater. 106 (2016) 66–77.
[34] G. Bonny, et al., Model. Simul. Mater. Sci. Eng. 19 (8) (2011) 085008.